WATER RESOURCES RESEARCH, VOL. 36, NO. 6, PAGES 1457–1465, JUNE 2000

Transport of polydisperse colloids in a saturated fracture with spatially variable aperture

Scott C. James and Constantinos V. Chrysikopoulos

Department of Civil and Environmental Engineering, University of California, Irvine

Abstract. A particle tracking model is developed to simulate the transport of variably sized colloids in a fracture with a spatially variable aperture. The aperture of the fracture is treated as a lognormally distributed random variable. The spatial fluctuations of the aperture are described by an exponential autocovariance function. It is assumed that colloids can sorb onto the fracture walls but may not penetrate the rock matrix. Particle advection is governed by the local fracture velocity and diffusion by the Stokes-Einstein equation. Model simulations for various realizations of aperture fluctuations indicate that lognormal colloid size distributions exhibit greater spreading than monodisperse suspensions. Both sorption and spreading of the polydisperse colloids increase with increasing variance in the particle diameter. It is shown that the largest particles are preferentially transported through the fracture leading to early breakthrough while the smallest particles are preferentially sorbed. Increasing the variance of the aperture fluctuations leads to increased tailing for both monodisperse and variably sized colloid suspensions, while increasing the correlation length of the aperture fluctuations leads to increased spreading.

1. Introduction

Studies of groundwater flow and contaminant transport in fractured media are of great interest to researchers investigating the storage of hazardous wastes in fractured subsurface formations. In many geologic formations with low matrix permeability, fluid flow occurs predominantly through fractures. Whether the flow takes place through a single fracture or through a network of fractures, it is important to fully understand fluid flow and contaminant transport through a single rough-walled fracture. Furthermore, there is considerable evidence that colloids can enhance contaminant transport in fractured media [*Abdel-Salam and Chrysikopoulos*, 1995a, b; *Ibaraki and Sudicky*, 1995]. However, it should be noted that colloids have transport properties that differ from those of solutes [*Abdel-Salam and Chrysikopoulos*, 1994; *Kessler and Hunt*, 1994; *Chrysikopoulos*, 1999].

Colloids are very fine particles such as minerals, metal oxides, viruses, bacteria, and organic macromolecules that range in size from 10^{-3} to 10 μm [*Chrysikopoulos and Sim*, 1996]. A wide variety of microorganisms, organic, and inorganic materials are present in groundwater and all can be considered colloidal. Colloids are often introduced in groundwater artificially through the injection of cementing or slurry agents, or mobilized during well installation and operation. Colloids have the potential to move through groundwater systems faster than nonsorbing solutes because their large size and low diffusivity tends to exclude them from regions of low groundwater velocities [*Bales et al*., 1989; *Grindrod*, 1993; *James and Chrysikopoulos*, 1999].

Colloids have high specific surface areas per unit mass (values as high as 300 m^2/g have been reported by *Chung and Lee* [1992]); thus they possess a high sorptive capacity for contaminants and are themselves readily able to sorb onto solid surfaces. The adsorption process of colloids onto solid surfaces is often termed as deposition, attachment, or filtration. Deposition of colloids is affected by Brownian motion, the repulsive electric double layer, attractive van der Waals forces, and solution chemistry [*Payatakes et al*., 1974]. Particle deposition is also affected by whether fracture surfaces are clean or deposition occurs onto previously deposited particles. Detachment of colloids is not expected in fractures where flow velocities are low. *Bowen and Epstein* [1979] have shown experimentally that the release rate of deposited colloids from a smooth parallel plate channel is negligible and in many studies colloid deposition is considered irreversible [e.g., *Elimelech et al*., 1995, p. 411; *Johnson et al*., 1996]. Colloid deposition onto a solid surface is often modeled as a kinetic sorption process and by the Smulochowski-Levich perfect sink approximation [*James and Chrysikopoulos*, 1999]. In this study a kinetic sorption model, which specifically tracks particle-wall collisions, will be employed.

Available experimental data indicate that colloids found in natural environments typically follow a lognormal distribution in diameter [*Ledin et al*., 1994]. A variability in diameter alone is enough to influence transport properties. *James and Chrysikopoulos* [1999] have shown that lognormal colloid size distributions exhibit greater spreading than monodisperse suspensions being transported in a single, one-dimensional, uniform fracture. Furthermore, it was shown that larger particles are least retarded and smaller particles are more slowly transported. In this study we extend our previous research efforts in order to investigate the transport of polydisperse colloid distributions in a two-dimensional fracture with variable aperture under both sorbing and nonsorbing conditions.

2. Fracture Generation

Figure 1 is an illustration of the system modeled in this work. The two-dimensional fracture used in this study is 8 m long (x

Paper number 2000WR900048.
0043-1397/00/2000WR900048$09.00

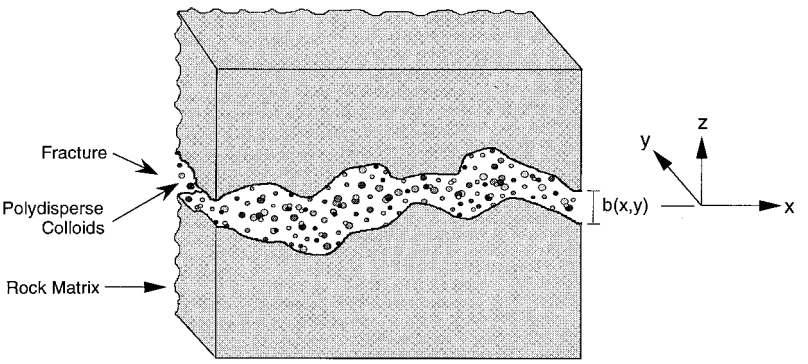

Figure 1. Schematic illustration of a two-dimensional fracture with spatially variable aperture $b(x, y)$ and a migrating plume of polydisperse colloids undergoing surface sorption. Note that $z = 0$ at the center of the fracture.

direction) and 4 m wide (y direction). The fracture plane is partitioned into 3200 discrete square elements as illustrated in Figure 2. Each 10×10 cm unit element exhibits a distinct aperture. The aperture field in the fracture is generated stochastically by the geostatistical code SPRT2D [*Gutjahr*, 1989]. It is assumed that the aperture distribution in the fracture plane follows a lognormal distribution [*Johns et al*., 1993; *Reimus et al*., 1993; *Keller*, 1998] with preselected mean and variance. Furthermore, the aperture distribution was assumed to vary spatially according to an isotropic exponential autocovariance function with specified correlation length. By definition, a correlation length implies that for distances in the fracture plane smaller than the correlation length the aperture values are likely to be similar, but at distances larger than the correlation length there is no correlation between apertures at different locations. Unique realizations of the aperture field are obtained by changing the seed number of the random field generator.

3. Flow in a Fracture

3.1. Mathematical Model

The two-dimensional, steady state partial differential equation describing flow in a spatially variable fracture is [*Chrysikopoulos and Abdel-Salam*, 1997]

$$\frac{\partial}{\partial x}\left[b^3(x, y)\,\frac{\partial h(x, y)}{\partial x}\right] + \frac{\partial}{\partial y}\left[b^3(x, y)\,\frac{\partial h(x, y)}{\partial y}\right] = 0, \quad (1)$$

where $b(x, y)$ is the local fracture aperture and h is the piezometric head. The preceding equation assumes that the cubic law (Reynolds equation) for incompressible laminar flow between two parallel plate elements can effectively simulate the average flow at every point within the fracture. The above equation is a stochastic partial differential equation because one of its parameters, namely $b(x, y)$, is a stochastic variable. It should be noted that *Brown et al*. [1995] have shown that the cubic law tends to overestimate fluid velocity in low aperture

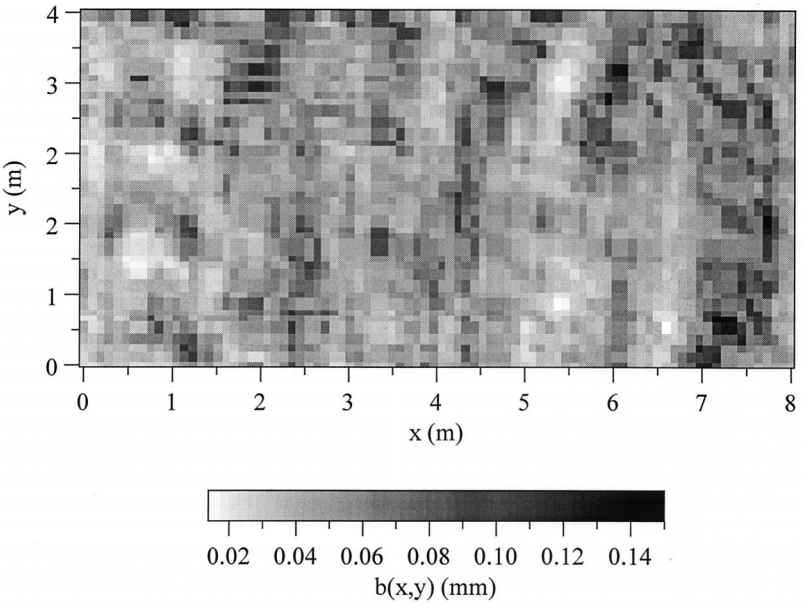

Figure 2. A realization of the aperture spatial distribution in the fracture plane. The fracture is partitioned into 80×40 equal-size elements. The coded scale illustrates apertures between 0.01 and 0.15 mm (here $x = 8.0$ m, $y = 4.0$ m, $\bar{b} = 5 \times 10^{-5}$ m, $\sigma^2_{\ln b} = 0.15$, and $\xi = 1$ m).

areas. However, flow through variable aperture fractures has been shown to follow preferential flow channels [*Abdel-Salam and Chrysikopoulos*, 1995a]. Consequently, the overall error introduced by the assumed cubic law approximation is relatively small.

For each realization of the aperture field a distribution of the piezometric head within the fracture is obtained by solving the governing fluid flow equation (1) subject to constant head (Dirichlet) boundary conditions along the $x = 0$ and $x = 8$ m sides of the fracture. A net flow is induced in the positive x direction with the incorporation of no-flow (Neumann) boundary conditions along the sides of the fracture at $y = 0$ and $y = 4$ m. Flow in the rock matrix is neglected because the saturated hydraulic conductivity in the rock matrix is several orders of magnitude smaller than the saturated hydraulic conductivity in the fracture [*Abdel-Salam and Chrysikopoulos*, 1996]. A grid of 3321 (81×41) nodes is laid over the two-dimensional fracture (system of elements) considered here, and the piezometric head is determined at each node.

3.2. Numerical Formulation

The equivalent aperture between adjacent elements in the x and y directions is obtained by employing the harmonic mean [*Reimus*, 1995]. Using a five-point central finite difference numerical approximation for the solution of the governing flow equation for each node on the grid of the fracture plane results in a set of linear equations with as many unknowns as the number of unspecified nodes on the fracture grid [*Hoffman*, 1992, p. 825]. The resulting set of linear equations is solved using a banded LU decomposition matrix solver algorithm [*Press et al*., 1992, p. 963]. Average velocity components in the x and y directions are then calculated for every unit element from the steady state volumetric fluxes by the following expressions:

$$\bar{U}_x = -\frac{\gamma b^2(x, y)}{12\eta}\frac{\partial h(x, y)}{\partial x}, \tag{2a}$$

$$\bar{U}_y = -\frac{\gamma b^2(x, y)}{12\eta}\frac{\partial h(x, y)}{\partial y}, \tag{2b}$$

where γ is the fluid specific weight and η is the fluid dynamic viscosity. Second-order accurate finite difference forms of (2a) and (2b) are used in this analysis. Because a parabolic velocity profile develops within each element, the velocities in the x and y directions are functions of z and can be expressed as

$$U_x(x, y, z) = \bar{U}_x(x, y)\,\frac{3}{2}\left\{1 - 4\left[\frac{z}{b(x, y)}\right]^2\right\}, \tag{3a}$$

$$U_y(x, y, z) = \bar{U}_y(x, y)\,\frac{3}{2}\left\{1 - 4\left[\frac{z}{b(x, y)}\right]^2\right\}, \tag{3b}$$

where z is the direction normal to the fracture surface. Equations (3a) and (3b) are consequences of the no slip boundary conditions at the fracture walls, and they are spatial functions of the (x, y, z) location in the fracture.

4. Algorithm Development

4.1. Particle Tracking

A particle tracking technique is used for the colloid transport problem instead of a finite difference or a finite element solution method because of the irregular boundaries of the variable aperture fracture as well as the polydisperse colloid distributions. Particle tracking algorithms are stochastic solutions to linear partial differential equations which do not provide direct numerical solutions and therefore do not suffer from numerical dispersion as do the finite element and finite difference methods [*Thompson and Gelhar*, 1990]. Each particle is individually considered (i.e., stored in a memory location), thus retaining its own unique characteristics including, for example, size and sorption status.

Particle tracking techniques have been frequently applied to investigations of contaminant transport in porous and fractured media [*Smith and Schwartz*, 1980; *Kinzelbach and Uffink*, 1988; *Chrysikopoulos et al*., 1992; *Thompson et al*., 1996; *James and Chrysikopoulos*, 1999]. The general particle tracking transport equation consists of an absolute term, in this case due to advection; and a stochastic term representing the random molecular diffusion [*Thompson*, 1993; *Kitanidis*, 1994]. In vector notation the particle tracking equation is given by [*Thompson and Gelhar*, 1990]

$$\mathbf{X}^m = \mathbf{X}^{m-1} + \mathbf{A}(\mathbf{X}^{m-1})\Delta t + \mathbf{B}(\mathbf{X}^{m-1}) \cdot \mathbf{Z}\sqrt{\Delta t}, \tag{4}$$

where exponent m is the numerical step number, $\mathbf{X}^m$ is the three-dimensional position vector at time level $m\Delta t$; $\mathbf{A}(\mathbf{X}^{m-1})$ is the absolute forcing vector (i.e., the velocity profile) evaluated at $\mathbf{X}^{m-1}$; $\mathbf{B}(\mathbf{X}^{m-1})$ is a deterministic scaling second-order tensor evaluated at $\mathbf{X}^{m-1}$ (i.e., a function of the molecular diffusion coefficient); and $\mathbf{Z}$ is a vector of three independent normally distributed random numbers with zero mean and unit variance. The terms of the diagonal second-order tensor $\mathbf{B}(\mathbf{X}^{m-1})$ are equal to $\sqrt{2\mathcal{D}}$ [*Ahlstrom et al*., 1977]. The molecular diffusion coefficient $\mathcal{D}$ is given by the Stokes-Einstein equation as

$$\mathcal{D} = \frac{kT}{3\pi\eta d_p}, \tag{5}$$

where k is Boltzmann's constant; d_p is the particle diameter; and T is the absolute temperature of the solvent (water). In view of (3a) and (3b), (4), and (5), the overall transport equations for the problem examined in this work can be written as

$$x^m = x^{m-1} + \bar{U}_x(x^{m-1}, y^{m-1})\,\frac{3}{2}\left\{1 - 4\left[\frac{z^{m-1}}{b(x, y)}\right]^2\right\}\Delta t + Z_1\sqrt{2\mathcal{D}\Delta t}, \tag{6}$$

$$y^m = y^{m-1} + \bar{U}_y(x^{m-1}, y^{m-1})\,\frac{3}{2}\left\{1 - 4\left[\frac{z^{m-1}}{b(x, y)}\right]^2\right\}\Delta t + Z_2\sqrt{2\mathcal{D}\Delta t}, \tag{7}$$

$$z^m = z^{m-1} + Z_3\sqrt{2\mathcal{D}\Delta t}. \tag{8}$$

In order to account for surface sorption, knowledge of exactly where and when a particle hits a wall is required. Only if extremely small time steps are taken (small time steps are computationally costly) can (4) accurately account for each wall collision. Instead, a characteristic spatial step in the z direction was specified, and the associated time for the particle to travel this distance was determined. The time required for a particle to move a specified distance in the z direction, $\Delta z = z^m - z^{m-1}$, is given by [*Reimus*, 1995, p. 96]

$$\Delta t = \exp\left\{\ln\left[\frac{(\Delta z)^2}{2\mathcal{D}}\right] - 0.2 + 0.79Z_3\right\}. \tag{9}$$

The preceding expression was developed by fitting the distribution of log times required for particles to move a specified

distance Δz, according to (4) with numerous very small Δt values. These normally distributed log times consistently had a mean of $\ln[(\Delta z)^2/2\mathcal{D}] - 0.2$ with standard deviation 0.79. Once the time step associated with a particle's movement of Δz is determined from (9), the corresponding distances moved by the particle in the x and y directions are determined from (6) and (7), respectively. Although the vertical spatial increment is specified before a particle is moved, the vertical direction (up or down) that the particle follows is determined by the sign of a randomly selected number from a normal distribution with mean zero and variance one. It should be noted that factors such as gravity, clogging, and filtration can affect colloid transport in fractures; however, they have not been accounted for in the present study in the interest of simplicity and in order to explicitly examine ideal particle transport and sorption in a variable aperture fracture.

4.2. Numerical Methods

A large number of particles (10,000 colloids) is employed for the model simulations in order to reduce random noise. Although by increasing the number of particles more computation time is required, a large number of particles leads to smoother results by averaging out the effect of an individual particle. As in any averaging process, the larger the sample size, the smaller the contribution of a single component and the smoother the results.

The colloids are introduced at the inlet side of the fracture flow domain ($x = 0$) and distributed according to the local volumetric flow rate as suggested by *Reimus* [1995, p. 93]. A discrete cumulative probability density function based on the volumetric flow rate into each inlet unit element of the fracture is constructed by summing all individual element flow rates at the fracture inlet and determining each element's contribution (probability) to the total sum. Subsequently, a uniform random number between zero and one is generated for each particle. The random number's placement in the cumulative distribution of the flow rates at the inlet designates the corresponding entrance unit element. Furthermore, it is assumed that the probability of a colloid entering a designated unit element of the fracture inlet at a given z location (perpendicular to the fracture walls) is proportional to the flow rate at that particular position. Consequently, the probability of a colloid having a starting position less than z is given by [*Reimus*, 1995]

$$P(z) = \frac{\int_{-b/2}^{z} U_x(0, y, z)dz}{\int_{-b/2}^{b/2} U_x(0, y, z)dz}. \tag{10}$$

Substituting (3a) into (10) and integrating yields the following cubic equation:

$$P(z) = -\frac{2z^3}{b^3(0, y)} + \frac{3z}{2b(0, y)} + \frac{1}{2}. \tag{11}$$

A uniform random number between zero and one is substituted for $P(z)$ in (11) and the roots of the resulting polynomial in z are evaluated by Newton's method. Roots found outside of the range of $-b(0, y)/2$ and $b(0, y)/2$ are ignored.

For an impermeable solid matrix, if not sorbed, all particles are assumed to be reflected from fracture walls as in a mirror image without loss of energy. That is, the final x and y coordinates position remain unchanged, whereas the final z coordinate is set at a distance away from the wall equal to the distance that the particle would have obtained if it had penetrated the rock matrix. For example, if z initially obtained a value of 5.03×10^{-5} m (5.0×10^{-5} m being the location of the fracture wall), its reflected z location would be 4.97×10^{-5} m.

Particle movements between elements of different aperture is assumed to follow the relationship [*Happel and Brenner*, 1965, p. 553]

$$\frac{z_{\text{old}}}{b_{\text{old}}} = \frac{z_{\text{new}}}{b_{\text{new}}}, \tag{12}$$

which is applicable for creeping flow conditions in slowly converging or diverging channels. Thus the ratio of the new z location to the old z location is equivalent to the ratio of the fracture aperture at the new location to the fracture aperture at the old location. Particles are allowed to cross both perpendicularly as well as diagonally between elements. In either case only the initial and final element apertures are used in (12).

5. Particle Deposition

The transport of colloids in fractured media is significantly affected by colloid deposition onto formation surfaces. As a colloid travels through a fracture, the transport mechanisms (advection and diffusion) may eventually bring the particle close enough to the aperture surface to have the opportunity to establish a fracture wall contact. Colloid attachment mechanisms are mainly dominated by repulsive electrostatic, attractive van der Waals, and hydrodynamic forces [*McDowell-Boyer et al.*, 1986]. The probability of a particle sorbing per wall collision (attachment efficiency) is calculated by a modified Boltzmann law equation

$$p = \exp\left[\frac{-\phi}{kT}\right] F(n^*), \tag{13}$$

where ϕ is the repulsive energy of interaction of the particle with the fracture surface ($\phi \simeq 10kT$ [*Adamczyk et al.*, 1997]) and $F(n^*)$ is the dynamic blocking function (DBF) which takes into account the effect of previously deposited particles per unit fracture surface area, n^*, on subsequent colloid deposition by specifying the portion of the fracture surface area that remains available for deposition [*Chrysikopoulos and Abdel-Salam*, 1997]. The Boltzmann law assumes that if a particle comes into contact with a fracture wall, it is either adsorbed with probability p or reflected. For example, if $\phi = 10kT$ and the fracture surface is free of previously deposited colloids, then according to (13), $p = 4.54 \times 10^{-5}$, and roughly two particles per every 10^4 wall collisions will sorb onto the fracture surface. The modified Boltzmann law, (13) is incorporated into the particle tracking simulation as follows: each time a particle-wall encounter is recorded, first the probability p is determined, and then a uniform random number between zero and one is generated. Particle attachment is assumed to occur if the selected random number is less than or equal to p.

Particles accumulated on fracture surfaces influence the adsorption of other particles in their vicinity due to geometric volume exclusion. Desorption is often assumed to be negligible [*Bowen and Epstein*, 1979]. The effect of previously deposited colloids can be taken into account through use of the DBF. The value of a DBF ranges between one (for a fracture free of colloids) and zero (for a fracture surface completely covered by

deposited colloids). When interstitial fluid and sorbent surface chemical conditions favor the attachment of stable colloid particles onto sorbent surfaces, colloid deposition is essentially irreversible and restricted to monolayer coverage [*Johnson et al*., 1996]. For the case of irreversible sorption the linear DBF (the area that remains available for a colloid to deposit onto the fracture wall) is given by [*Song and Elimelech*, 1994; *Chrysikopoulos and Abdel-Salam*, 1997]

$$F(n^*) = \frac{\varepsilon_{\max} - \varepsilon}{\varepsilon_{\max}}; \tag{14}$$

where

$$\varepsilon(t, x, y) = A_p n^*(t, x, y); \tag{15}$$

and

$$\varepsilon_{\max} = 1/\beta; \tag{16}$$

where $A_p = \pi d_p^2/4$ is the cross-sectional area of a colloidal particle and β (≥ 1) is a dimensionless parameter representing the ratio of the fracture surface area blocked by a deposited colloidal particle to the projected area of the particle (excluded area or hydrodynamic shadow effect) [*Rajagopalan and Chu*, 1981]. Owing to electrostatic repulsive forces, a sorbed colloid effectively blocks more area than simply the space it physically occupies. Nonlinear DBFs have also been employed in studies of colloid transport in fractures [e.g., *Chrysikopoulos and Abdel-Salam*, 1997; *James and Chrysikopoulos*, 1999]; however, in this study only the linear DBF, (14), is examined.

6. Model Simulations

One monodisperse and three polydisperse colloid size distributions are examined here. All distributions have the same mean colloid diameter, $\mu = 1$ μm, whereas the three polydisperse colloid distributions are lognormal with variances of the colloid diameter, $\sigma_{d_p}^2 = 0.6$, 1.2, and 1.8 μm^2.

The hypothetical fracture used in this work is subjected to a hydraulic gradient of 0.031 along the x direction. Cumulative colloid mass M, passing across the fracture width at $x = 8$ m, normalized by the initial liquid phase colloid mass M_o, is evaluated by averaging the results from 50 realizations of the fracture aperture field. The number of realizations is chosen such that additional realizations do not change the calculated ensemble average by more than 2%. It should be noted that M is determined by summing the volume of colloids passing across the fracture width at $x = 8$ m and multiplying by the colloidal particle density, $\rho_p = 2000$ kg/m^3 [*McCarthy and Degueldre*, 1993, p. 247]. Furthermore, the spatial step in the z direction, Δz, is set equal to 1/20th of the local aperture. This distance was chosen in order to assure that a particle will not travel across multiple elements in either the x or y directions during a single time step.

Figure 3 qualitatively illustrates the effect of colloid diameter distribution, fracture aperture variability, and colloid sorption on the transport of 10,000 colloid particles in water-saturated fractures. Four different cases are considered when the colloids have been in the system for 17.5 hours. The first case (Figure 3a) represents a fracture with uniform aperture, $b = 5 \times 10^{-5}$ m, and a plume of monodisperse colloids with particle diameter $d_p = 1$ μm. The second case (Figure 3b) represents a fracture with uniform aperture ($b = 5 \times 10^{-5}$ m) and a plume of polydisperse colloids with lognormal diameter distribution described by a mean particle diameter $\mu = 1$ μm and variance $\sigma_{d_p}^2 = 1.8$ μm^2. It should be noted that this polydisperse plume is divided into three equally numbered groups based on diameter. The triangles represent the smallest third, the squares represent the middle third, and the circles represent the largest third. The next case (Figure 3c) represents a fracture with mean aperture $\bar{b} = 5 \times 10^{-5}$ m, variance of the log-transformed spatially variable aperture $\sigma_{\ln b}^2 = 0.037$, correlation length of the aperture $\xi = 1$ m, and the identical plume of polydisperse colloids used in the previous case. Finally, the last case (Figure 3d) represents the same situation as the third case with the additional constraint that the polydisperse colloids may undergo irreversible sorption. It should be noted that colloids sorbed onto the fracture surfaces as well as colloids in suspension are presented in Figure 3d with sorbed colloids having their respective solid symbol. Comparison of the four cases reveals that polydisperse colloid suspensions spread more within the fracture than monodisperse suspensions (see Figures 3a and 3b); larger colloids breakthrough first (see Figure 3b); aperture variability leads to preferential flow paths (see Figure 3c); and that the smallest colloids of the plume are preferentially sorbed as more of the smaller than the larger colloids are shown attached (Figure 3d).

Normalized colloid mass breakthrough curves of the four colloid plumes considered in this study are presented in Figure 4 for the case of transport in a uniform fracture. Clearly, the earliest colloid mass breakthrough corresponds to the plume with the largest $\sigma_{d_p}^2$. As illustrated in Figure 3b, colloid separation within a plume is based on particle diameter size with the larger colloids traveling faster than the smaller colloids. Large colloids, due to their size, are physically excluded from the slowest moving portion of the velocity profile nearest to the wall. Furthermore, large particles remain in high-velocity streamlines in the center of the fracture longer than the small particles due to their lower diffusivity. Consequently, the largest particles travel at a velocity somewhat higher than the mean fluid velocity. *McTigue et al*. [1986] suggested that large particles tend to remain in high-velocity streamlines near the center of the fracture longer than small particles because of fluid-particle phases stresses, drag, lift, and Faxen forces. It should be noted that these effects have not been accounted for in the present analysis.

The effect of the variance of the log-transformed aperture on the transport of polydisperse colloids in fractures with spatially variable aperture is shown in Figure 5. Four different $\sigma_{\ln b}^2$ values are examined: 0.0, 0.007, 0.037, and 0.125. Comparison of the normalized colloid mass breakthrough curves indicate that increasing $\sigma_{\ln b}^2$ increases the tailing of the colloid plume. It is well established in the literature that increasing the heterogeneity of any flow or transport parameter leads to increased spreading [e.g., *Dagan*, 1982; *Chrysikopoulos*, 1995]. Although the fracture was considered impermeable in this work, it has been shown that matrix diffusion leads to increased retardation as well as increased tailing [*James and Chrysikopoulos*, 1999]. *Rehmann et al*. [1999] have suggested that premature breakthrough of viruses (acting like colloids) in highly heterogeneous porous media is a result of the presence of preferential flow paths. Similarly, the results of this study indicate that portions of the fracture with large aperture allow for early colloid breakthrough while the many portions of the fracture with small aperture contribute to increased tailing by slowing colloids. It should be noted that flow through small apertures can be overestimated by the cubic law approximation

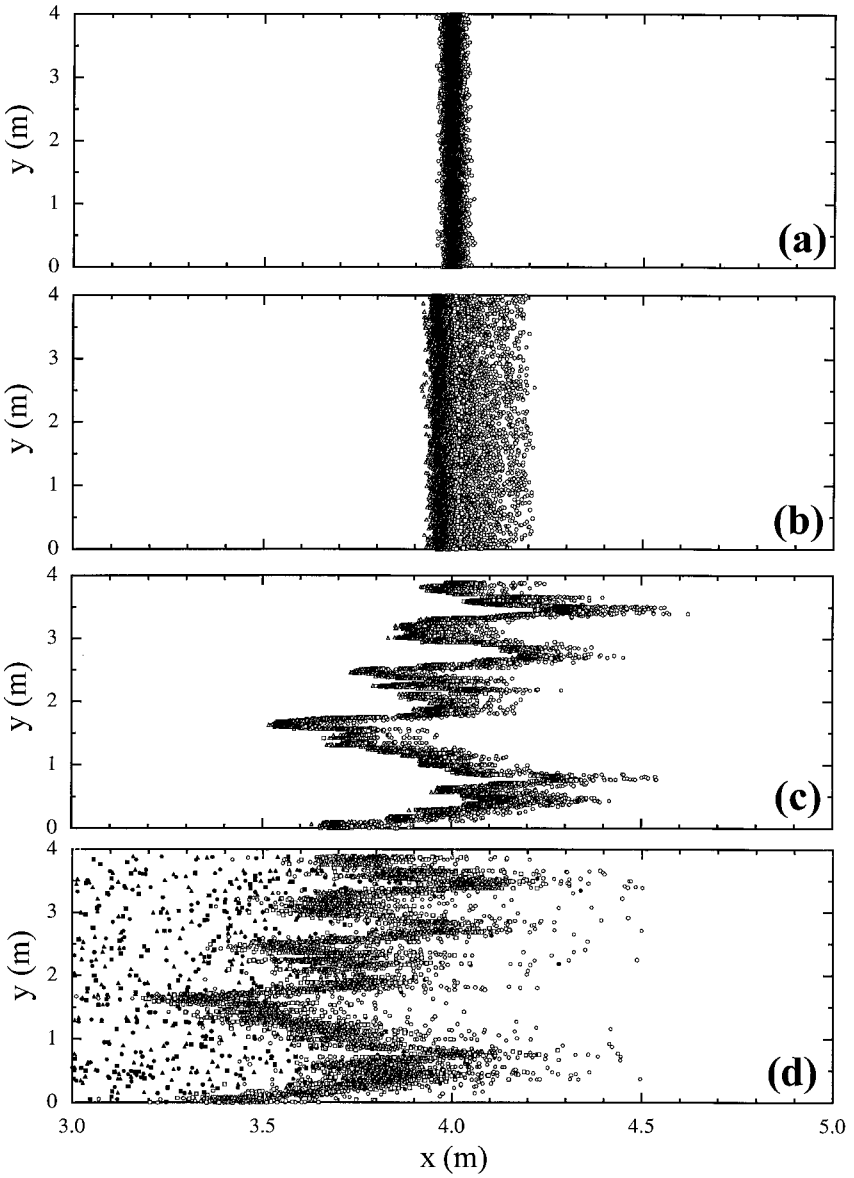

Figure 3. Snapshots of colloid positions for (a) a monodisperse colloid plume in a uniform aperture fracture; (b) a polydisperse colloid plume in a uniform aperture fracture; (c) a polydisperse colloid plume in a variable aperture fracture; and (d) a polydisperse colloid plume undergoing sorption in a variable aperture fracture. The polydisperse colloid plumes are split into third based on particle sizes with triangles being the smallest third, squares being the middle third, and circles being the largest third. Sorbed colloids are represented by the respectively solid symbols (here $t = 17.5$ hours, flow direction from left to right).

[*Brown et al*., 1995]. Consequently, experimental data from studies of colloid transport in fractures with variable aperture may exhibit even greater tailing than what is predicted by the present model. Although some experiments for colloid transport in fractures are presented in the literature [e.g., *Bales et al*., 1989], the available experimental data cannot be directly compared with the particle tracking model presented here because several of the required model parameters are not provided.

The effect of the correlation length of aperture fluctuations on polydisperse colloid transport in a fracture with variable aperture is illustrated in Figure 6. The simulated normalized breakthrough curves indicate that colloid spreading increases with increasing ξ. Consequently, the longitudinal dispersivity of a fracture with spatially variable aperture is proportional to ξ and $\sigma^2_{\ln b}$. This is analogous to the increase in dispersivity for a heterogeneous porous medium caused by an increase in the variance and correlation length of the hydraulic conductivity [*Gelhar and Axness*, 1983].

Figure 7 illustrates the effect of irreversible sorption on polydisperse colloid transport in a variable aperture fractures. Sorption causes reduction in the number of colloids suspended in the liquid phase prohibiting the normalized breakthrough curves from reaching the maximum value of one. These results are in agreement with previous investigations by *Abdel-Salam and Chrysikopoulos* [1994]. However, it is worthwhile to note that increasing $\sigma^2_{\ln b}$ leads to elongated tailing of the colloid plume as well as enhanced colloid deposition. This result is attributable to the fact that for lognormally distributed apertures, a long tail toward larger aperture exists with the majority

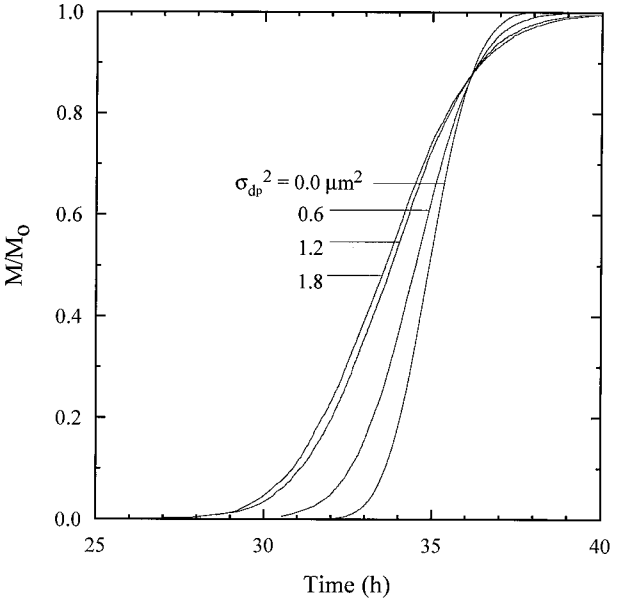

Figure 4. Normalized mass breakthrough curves for a monodisperse and three polydisperse colloid plumes with mean diameter $\mu = 1$ μm in a uniform fracture with aperature $b(x, y) = 5 \times 10^{-5}$ m.

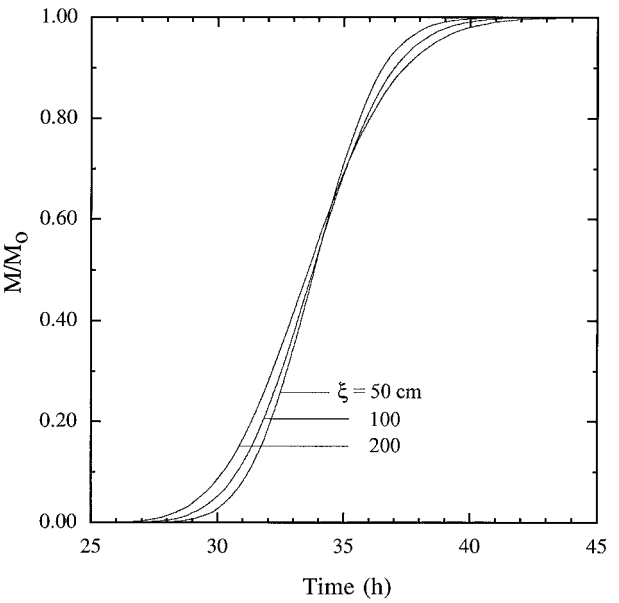

Figure 6. Normalized mass breakthrough curves for a polydisperse colloid plume in variable aperture fractures with three different correlation lengths of the aperture fluctuations (here $\bar{b} = 5 \times 10^{-5}$ m, $\sigma^2_{\ln b} = 0.037$, $\mu = 1$ μm, $\sigma^2_{d_p} = 1.8$ μm^2.

of the aperture below the mean. As $\sigma^2_{\ln b}$ increases, the difference between the largest and the smallest aperture increases as does the area of small aperture. With an increased area of small aperture, more particle-wall collisions are expected which in turn lead to increased colloid sorption. Furthermore, it is clear from Figure 3d that, on average, it is the largest particles which travel farther through the fracture and the smallest ones which are being deposited. Small particles have higher molecular diffusion coefficient than large particles, thus small particles encounter the wall more frequently resulting in increased attachment.

7. Summary

The transport of polydisperse colloid plumes in a water-saturated fracture with spatially variable aperture was modeled with a particle tracking technique. Results from model simulations show that polydisperse colloid suspensions exhibit different transport characteristics than monodisperse suspensions. The observed spreading of colloid plumes can be attributed to variability in both fracture aperture fluctuations as well as colloid diameters. Small colloids tend to travel at

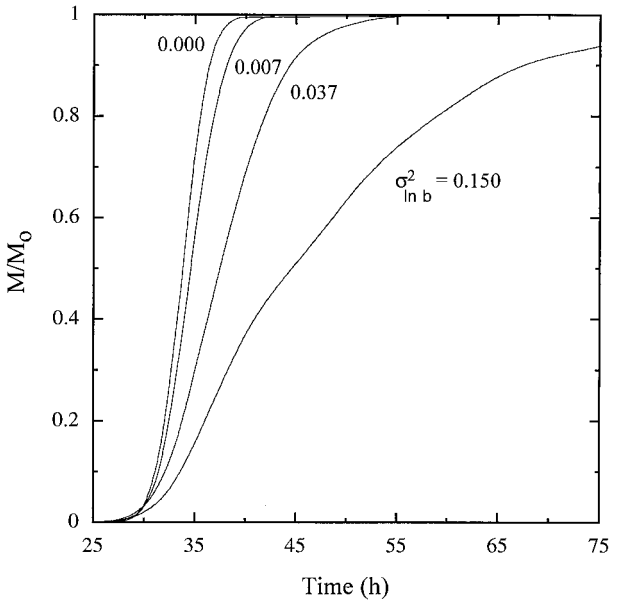

Figure 5. Normalized mass breakthrough curves for a polydisperse colloid plume in variable aperture fractures with four different $\sigma^2_{\ln b}$ values (here $\bar{b} = 5 \times 10^{-5}$ m, $\sigma^2_{d_p} = 1.2$ μm^2, $\mu = 1$ μm, $\xi = 1$m).

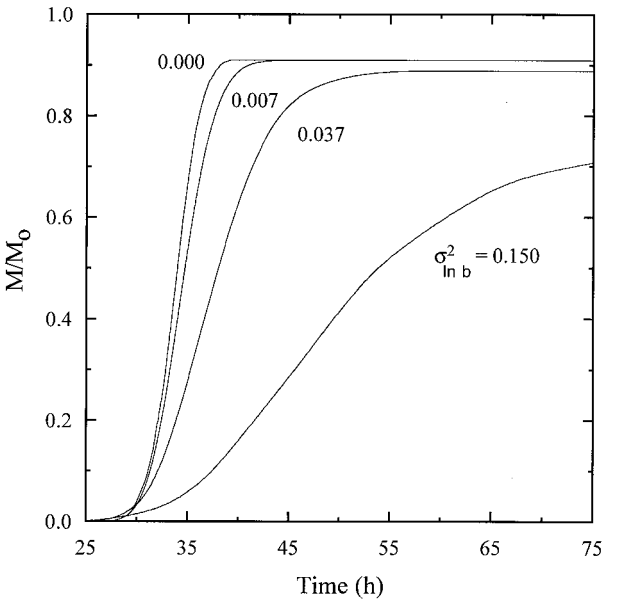

Figure 7. Normalized mass breakthrough curves for an irreversibly sorbing polydisperse colloid plume in variable aperture fractures with four different $\sigma^2_{\ln b}$ values (here $\bar{b} = 5 \times 10^{-5}$ m, $\sigma^2_{d_p} = 1.2$ μm^2, $\mu = 1$ μm, $\xi = 1$ m, $\phi = 10kT$, $\beta = 15$).

velocities closer to the mean flow velocity, while larger colloids can travel slightly faster, effectively increasing the spreading of the plume. Increasing the variability and/or the correlation length of the fracture aperture fluctuations, more spreading of the colloids is observed. When surface sorption is accounted for, it is the smallest colloids of a plume which are preferentially sorbed.

8. Notation

A_p projected (cross-sectional) area of a colloidal particle: $\pi d_p^2/4$ (L^2).
A absolute forcing vector (Lt^{-1}).
b local aperture (L).
$\bar{b}$ mean fracture aperture (L).
B deterministic scaling tensor $(Lt^{-1/2})$.
d_p diameter of a colloid particle (L).
$\mathcal{D}$ molecular diffusion coefficient (L^2t^{-1}).
$F(n^*)$ dynamic blocking function.
h piezometric head (L).
k Boltzmann's constant $(ML^2t^{-2}T^{-1})$.
m time step number.
M cumulative colloid mass passing through a cross section of the fracture (M).
M_o initial mass of suspended colloids (M).
n^* colloid number concentration deposited per unit fracture surface area (L^{-2}).
p probability of sorption from a modified Boltzmann law.
$P(z)$ probability of a colloid's inlet vertical location $<z$.
T absolute temperature of the solvent (T).
U_x parabolic flow velocity in the x direction (Lt^{-1}).
$\bar{U}_x$ average flow velocity in the x direction (Lt^{-1}).
U_y parabolic flow velocity in the y direction (Lt^{-1}).
$\bar{U}_y$ average flow velocity in the y direction (Lt^{-1}).
x coordinate along the fracture length (L).
X three-dimensional position vector (L).
y coordinate along the fracture width (L).
z coordinate perpendicular to the fracture plane (L).
Δz specified z direction spatial increment (L).
Z_1, Z_2, Z_3 randomly generated normally distributed numbers with zero mean and unit variance.
Z three-dimensional vector of randomly generated normally distributed numbers with zero mean and unit variance.

Greek letters

β scaling factor for fracture surface area blocked by a deposited colloid particle.
γ fluid specific weight $(ML^{-2}t^{-2})$.
Δt time step (t).
ε fraction of a fracture surface area covered (blocked) by deposited colloids.
$\varepsilon_{\max}$ fraction of a fracture surface area covered (blocked) by deposited colloids when n^* reaches its maximum.
η dynamic viscosity of the interstitial fluid $(ML^{-1}t^{-1})$.
μ mean colloid diameter (L).
ξ correlation length of the aperture fluctuations (L).
ρ_p colloid particle density (ML^{-3}).
$\sigma^2_{\ln b}$ variance of the log-transformed fracture aperture (L^2).
$\sigma^2_{d_p}$ variance of the colloid diameter distribution (L^2).
ϕ particle-wall repulsive interaction energy (ML^2t^{-2}).

Acknowledgments. This work was supported in part by the University of California, Irvine, through an allocation of computer resources on the SPP2000.

References

Abdel-Salam, A., and C. V. Chrysikopoulos, Analytical solutions for one-dimensional colloid transport in saturated fractures, *Adv. Water Resour.*, *17*, 283–296, 1994.

Abdel-Salam, A., and C. V. Chrysikopoulos, Modeling of colloid and colloid-facilitated contaminant transport in a two-dimensional fracture with spatially variable aperture, *Transp. Porous Media*, *20*, 197–221, 1995a.

Abdel-Salam, A., and C. V. Chrysikopoulos, Analysis of a model for contaminant transport in a fractured media in the presence of colloids, *J. Hydrol.*, *165*, 261–281, 1995b.

Abdel-Salam, A., and C. V. Chrysikopoulos, Unsaturated flow in a quasi-three-dimensional fractured medium with spatially variable aperture, *Water Resour. Res.*, *32*(6), 1531–1540, 1996.

Adamczyk, Z., B. Siwek, M. Zembala, and P. Weronski, Influence of polydispersity on random sequential adsorption of spherical particles, *J. Colloid Interface Sci.*, *185*, 236–244, 1997.

Ahlstrom, S. W., H. P. Foote, R. C. Arnett, C. R. Cole, and R. J. Serne, Multicomponent mass transport model: Theory and numerical implementation (discrete-parcel-random-walk version), Atl. Richfield Hanford Co., Richland, Wash., 1977.

Bales, R. C., C. P. Gerba, G. H. Grondin, and S. L. Jensen, Bacteriophage transport in sandy soil and fractured tuff, *Appl. Environ. Microbiol.*, *55*(8), 2061–2067, 1989.

Bowen, D. D., and N. Epstein, Fine particle deposition in smooth parallel plate channels, *J. Colloid Interface Sci.*, *72*, 81–97, 1979.

Brown, S. R., H. W. Stockman, and S. J. Reeves, Applicability of the Reynolds equation for modeling fluid flow between rough surfaces, *Geophys. Res. Lett.*, *22*(18), 2537–2540, 1995.

Chrysikopoulos, C. V., Effective parameters for flow in saturated heterogeneous porous media, *J. Hydrol.*, *170*, 181–198, 1995.

Chrysikopoulos, C. V., Transport of colloids in saturated fractures, in *Advances in Fracture Mechanics: Fractured Rock*, chap. 10, pp. 297–330, edited by M. H. Aliabadi, Comput. Mech., Billerica, Mass., 1999.

Chrysikopoulos, C. V., and A. Abdel-Salam, Modeling colloid transport and dispersion in saturated fractures, *Colloids Surf. A*, *121*, 189–202, 1997.

Chrysikopoulos, C. V., and Y. Sim, One-dimensional virus transport in homogeneous porous media with time dependent distribution coefficient, *J. Hydrol.*, *185*, 199–219, 1996.

Chrysikopoulos, C. V., P. K. Kitanidis, and P. V. Roberts, Generalized Taylor-Aris moment analysis of the transport of sorbing solutes through porous media with spatially-periodic retardation factor, *Transp. Porous Media*, *7*, 163–185, 1992.

Chung, J. Y., and K. J. Lee, Analysis of colloid transport and colloidal size effect using filtration theory, *Ann. Nucl. Energy*, *19*(3), 145–153, 1992.

Dagan, G., Analysis of flow through heterogeneous random aquifers, 2, Unsteady flow in confined formations, *Water Resour. Res.*, *18*(5), 1571–1585, 1982.

Elimelech, M., J. Gregory, X. Jia, and R. Williams, *Particle Deposition & Aggregation: Measurement, Modeling and Simulation*, 411 pp., Butterworth-Heinemann, Woburn, Mass., 1995.

Gelhar, L. W., and C. L. Axness, Three-dimensional stochastic analysis of macrodispersion in aquifers, *Water Resour. Res.*, *19*(1), 161–180, 1983.

Grindrod, P., The impact of colloids on the migration and dispersal of radionuclides within fractured rock, *J. Contam. Hydrol.*, *13*, 167–181, 1993.

Gutjahr, A. L., Fast Fourier transform for random field generation, project report, N. M. Inst. of Min. and Technol., Socorro, 1989.

Happel, J., and H. Brenner, *Low Reynolds Number Hydrodynamics*, 553 pp., Prentice-Hall, Englewood Cliffs, N. J., 1965.

Hoffman, J. D., *Numerical Methods for Engineers and Scientists*, 825 pp., McGraw-Hill, New York, 1992.

Ibaraki, M., and E. A. Sudicky, Colloid-facilitated contaminant transport in discretely fractured porous media, 1, Numerical formulation and sensitivity analysis, *Water Resour. Res*., *31*(12), 2945–2960, 1995.

James, S. C., and C. V. Chrysikopoulos, Transport of polydisperse colloid suspensions in a single fracture, *Water Resour. Res*., *35*(3), 707–718, 1999.

Johns, R. A., J. S. Steade, L. M. Costanier, and P. V. Roberts, Nondestructive measurements of fracture aperture in crystalline rock cores using X-ray computed tomography, *J. Geophys. Res*., *98*(B2), 1889–1900, 1993.

Johnson, R., S. Ning, and M. Elimelech, Colloid transport in geochemically heterogeneous porous media: Modeling and measurements, *Environ. Sci. Technol*., *30*, 3284–3293, 1996.

Keller, A. A., High resolution non-destructive measurement and characterization of fracture apertures, *Int. J. Rock Mech. Min. Sci*., *35*(8), 1037–1050, 1998.

Kessler, J. H., and J. R. Hunt, Dissolved and colloidal contaminant transport in a partially clogged fracture, *Water Resour. Res*., *30*(4), 1195–1206, 1994.

Kinzelbach, W., and G. J. M. Uffink, The random walk method in pollutant transport simulation, in *Groundwater Flow and Quality Modeling*, edited by E. Custodio et al., pp. 227–245, D. Reidel, Norwell, Mass., 1988.

Kitanidis, P. K., Particle-tracking equations for the solution of the advection-dispersion equation with variable coefficients, *Water Resour. Res*., *30*(11), 3225–3227, 1994.

Ledin, A., S. Karlsson, A. Duker, and B. Allard, Measurements in situ of concentration and size distribution of colloidal matter in deep groundwater by photon correlation spectroscopy, *Water Res*., *28*(7), 1539–1545, 1994.

McCarthy, J. F., and C. Degueldre, *Environmental Particles*, vol. 2, edited by J. Buffle and H. P. van Leeuwen, 247 pp., Lewis, Boca Raton, Fla., 1993.

McDowell-Boyer, L. M., J. R. Hunt, and N. Sitar, Particle transport through porous media, *Water Resour. Res*., *22*(13), 1901–1921, 1986.

McTigue, D. F., R. C. Gilver, and J. W. Nunziato, Rheological effects of nonuniform particle distributions in dilute suspensions, *J. Rheol*., *30*(5), 1053–1076, 1986.

Payatakes, A. C., C. Tien, and R. M. Turian, Trajectory calculation of particle deposition in deep bed filtration, part I, Model formulation, *AIChE J*., *20*(5), 889–900, 1974.

Press, W., S. Teukolsky, W. Vetterling, and B. Flannery, *Numerical Recipes in FORTRAN*, 963 pp., Cambridge Univ. Press, New York, 1992.

Rajagopalan, R., and R. Q. Chu, Dynamics of adsorption of colloidal particles in packed beds, *J. Colloid Interface Sci*., *86*, 299–317, 1981.

Rehmann, L. C., C. Welty, and R. W. Harvey, Stochastic analysis of virus transport in aquifers, *Water Resour. Res*., *35*(7), 1987–2006, 1999.

Reimus, P. W., The use of synthetic colloids in tracer transport experiments in a saturated rock fracture, *Rep. LA-13004-T*, Los Alamos Natl. Lab., Los Alamos, N. M., 1995.

Reimus, P. W., B. A. Robinson, and R. J. Glass, Aperture characteristics, saturated fluid-flow, and tracer transport calculations for a natural fracture, in *High-Level Radioactive Waste Management, Proceedings of the 4th Annual International Conference*, pp. 2009–2016, Am. Nucl. Soc., LaGrange Park, Ill., 1993.

Smith, L., and F. W. Schwartz, Mass transport, 1, A stochastic analysis of macrodispersion, *Water Resour. Res*., *16*(2), 303–313, 1980.

Song, L., and M. Elimelech, Transient deposition of colloidal particles in heterogeneous porous media, *J. Colloid Interface Sci*., *167*, 301–313, 1994.

Thompson, A. F. B., Numerical simulation of chemical migration in physically and chemically heterogeneous porous media, *Water Resour. Res*., *29*(11), 3709–3726, 1993.

Thompson, A. F. B., and L. W. Gelhar, Numerical simulation of solute transport in three-dimensional, randomly heterogeneous porous media, *Water Resour. Res*., *26*(10), 2541–2562, 1990.

Thompson, A. F. B., A. L. Schafer, and R. W. Smith, Impact of physical and chemical heterogeneity on cocontaminant transport in a sandy porous medium, *Water Resour. Res*., *32*(4), 801–818, 1996.

C. V. Chrysikopoulos (corresponding author) and S. C. James, Department of Civil and Environmental Engineering, University of California, Irvine, CA 92697-2175. (costas@eng.uci.edu; sjames@eng.uci.edu)

(Received July 7, 1999; revised February 14, 2000;
accepted February 22, 2000.)